Defense Technical Information Center
Compilation Part Notice

ADP012080

TITLE: Artificial Supercavitation. Physics and Calculation

DISTRIBUTION: Approved for public release, distribution unlimited

This paper is part of the following report:

TITLE: Supercavitating Flows [les Ecoulements supercavitants]

To order the complete compilation report, use: ADA400728

The component part is provided here to allow users access to individually authored sections of proceedings, annals, symposia, etc. However, the component should be considered within the context of the overall compilation report and not as a stand-alone technical report.

The following component part numbers comprise the compilation report:
ADP012072 thru ADP012091

Artificial Supercavitation. Physics and Calculation

Vladimir N. Semenenko
National Academy of Sciences - Institute of Hydromechanics
8/4 Zhelyabov str., Kyiv, 03057
Ukraine

Summary

This lecture is devoted to the basic physical properties and the calculation methods of the artificial cavitation (ventilation) flows. Main attention is paid to the three-dimensional ventilated supercavities past the disk and blunted cavitators.

Derivation of approximate equations of the axially symmetric supercavities with using the theorem of momentum and also the asymptotic theory of slender body is presented.

The G.V.Logvinovich independence principle of the cavity expansion is stated and grounded. It gives a simple and general method of investigating the unsteady problems.

Calculation of the ventilated cavities has some peculiarities caused by gravity effect, presence of the cavitator angle of attack and taking account of balance between the gas-supply into the cavity and the gas-leakage from the cavity. They are discussed here as well.

Introduction

The basic similarity parameter of cavitation flows is the cavitation number [1–4]:

$$\sigma = \frac{2(p_\infty - p_c)}{\rho V_\infty^2}, \tag{1}$$

where p_∞ is the pressure at infinity; p_c is the cavity pressure; ρ is the water density; V_∞ is the mainstream velocity. When a body moves horizontally on the immersion depth H, we have $p_\infty = \rho g H$, where g is the gravity acceleration. The supercavitation flow regime corresponds to small magnitudes $\sigma < 0.1$. When the magnitude of σ decreases, the supercavity dimensions increase.

When ρ = const, there are three possibilities of the σ reduction:

1) **Increasing the mainstream velocity** V_∞. With decreasing the mainstream velocity the rarefaction past bodies increases, and cavities are created by natural way when the pressure decreases to a value close to the saturated water vapor pressure p_v = 2350 Pascal (at the temperature 20 °C). Such supercavities are called the natural or vapor supercavities. The parameter

$$\sigma_v = \frac{2(p_\infty - p_v)}{\rho V_\infty^2} \tag{2}$$

is called the natural or vapor cavitation number. The natural supercavities are filled by water vapor under pressure $p_c = p_v$. The natural cavitation regime, when $\sigma_v < 0.1$, is attained when the mainstream velocity is very high: $V_\infty > 50$ m/sec.

Paper presented at the RTO AVT Lecture Series on "Supercavitating Flows", held at the von Kármán Institute (VKI) in Brussels, Belgium, 12-16 February 2001, and published in RTO EN-010.

2) **Decreasing the difference** $\Delta p = p_\infty - p_c$ owing to decreasing the ambient pressure p_∞, for example, in closed cavitation hydro-tunnels [4, 5]. The super-cavitation flows in the stream with artificially reduced pressure are sometimes called the artificial ones, although they do not distinguish on natural vapor supercavities by their physical properties.

3) **Decreasing the difference** $\Delta p = p_\infty - p_c$ owing to increasing the cavity pressure p_c. This is easy attained by blowing the air or another gas into the rarefaction zone past a non-streamlined body. Such supercavitation regime is called the artificial cavitation or ventilation. The method of obtaining the ventilated cavities was proposed independently by L.A.Epshtein and H.Reichardt in 1944 – 1945.

The ventilated cavitation regime σ < 0.1 is easy obtained at the significantly lower mainstream velocities V_∞ ~ 10 m/sec. That is why, it is widely applied in bench investigations of the supercavitation flows. The Fig. 1 presents a typical scheme of an experimental apparatus to investigate the ventilated cavities.

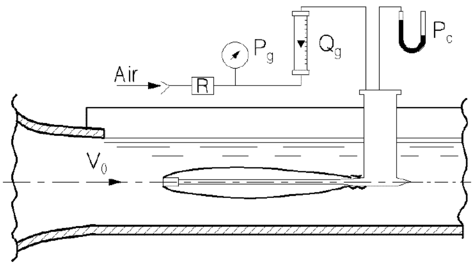

Fig. 1. Scheme of apparatus to create a ventilated supercavity

1 Main problems of artificial cavitation

It follows from the similarity theory of hydrodynamic flows [3] that the shape and dimensions of both the natural vapor supercavity and the artificial ventilated cavity must be the same when the cavity number is equal. However, in reality the full similarity does not fulfil due to a number of causes.

The main peculiarity of the artificial cavitation flows is a consequence of comparatively small values of the velocity $V = 10 \div 100$ m/sec. In this case the Froude number

$$Fr = \frac{V_\infty}{\sqrt{gD_n}} \tag{3}$$

where D_n is the cavitator diameter, has moderate magnitude.

This means that the gravity effect is considerably more for the artificial cavity when the cavitation number is the same. It causes to the more essential deformation of the artificial cavity shape. The floating-up the ventilated cavity tail may be essential so that it completely determines the cavity closure character and type of the gas leakage from the cavity.

Thus, the Froude number (3) together with the cavitation number (1) is the basic similarity parameter for the artificial supercavitation flows.

1.1 METHODS OF CREATION OF THE VENTILATED SUPER-CAVITIES

We know the following methods of creating the artificial ventilated cavities (Fig. 2):

1) **Method of a gas source** [6] consists in creating a gas envelope around a body by the air jet ejection from the body nose opposite to the stream (Fig. 2, a). It is obvious that in this case the gas pressure must exceed the pressure of the water in the nose stagnation point. From the Bernoulli equation [7], we obtain estimation of the necessary velocity of the air V_g :

$$V_g > V_\infty \sqrt{\frac{\rho}{\rho_g}(1+\sigma)} \approx 28.6\left(1+\frac{\sigma}{2}\right)V_\infty, \tag{4}$$

where ρ_g is the air density. One can see that the gas jet velocity and, hence, the gas rate must be very high.

Owing to the high velocity of the gas flow in the cavity, the cavity walls are strongly perturbed (the cavity is nontransparent). The flow represents a strongly turbulized two-phase zone at the tail cavity part and in the wake.

This way of the artifitial supercavity creation is not applied in practice due to its lacks.

2) **L.I.Sedov scheme** [7] consists in ejecting the slender water jet from the body nose opposite to the stream with simultaneous air-supply into the stagnation zone (so called "jet cavitator", Fig. 2, b). This flow scheme represents the inverted cavitation flow by Efros-Gilbarg with the reentrant jet [7]. The nose stagnation point is displaced into the stream, and in the ideal case of complete recovery of the pressure in the tail part, the body must suffer thrust

$$T = \rho S_j V_j V_\infty, \tag{5}$$

where S_j is the jet section area; V_j is the average velocity in the jet.

In real flows, it is impossible to attain smooth closure of the cavity on the body tail and complete recovery of the pressure. Therefore, the arising thrust will be smaller. Nevertheless, this scheme is very perspective. When $\sigma \to 0$, we obtain the infinite Kirchhoff's cavity. In this case the body with the jet cavitator suffers half drag in comparison with the body with the solid cavitator.

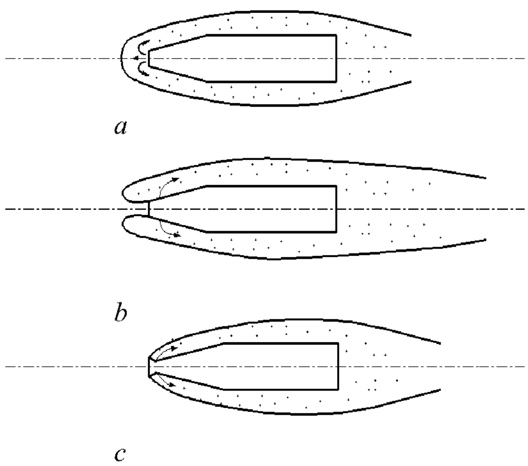

Fig. 2. Ways of creation of ventilated cavities: a – gas source; b – L.I.Sedov's scheme; c – blowing past a sharp edge

3) **Gas-supply past a sharp edge**. The most stable and smooth surface of the cavity is observed, if the cavity separation occurs on the sharp cavitator edge with simultaneous gas-supply to the separation place (Fig. 2, c). It is possible to supply gas in any point of the body after the fully development of the supercavity (so called "distributed gas-supply"). Experiments showed that location of the place of the gas-supply into the steady cavity has no essential significance.

The way of creation of ventilated cavities past cavitators with the sharp edge (for example a disk) is the most frequently used.

1.2 COEFFICIENT OF GAS-SUPPLY RATE INTO THE CAVITY

The main problem for the ventilated cavitation flows is a problem on the gas quantity necessary for supply into the cavity to maintain the supercavity of given dimension (i.e. to attain the given σ). In the case of axisymmetric cavitator, the dimensionless coefficient of the rate is introduced [2, 3]:

$$\overline{Q} = \frac{\dot{Q}}{V_\infty D_n^2}, \tag{6}$$

where $\dot{Q}$ is the volumetric gas rate at the pressure p_c, its dimensionality is m^3 / sec.

Obviously, the gas-supply rate $\dot{Q}_{in}$ must be equal to the gas-leakage rate $\dot{Q}_{out}$ when motion is steady. For unsteady ventilated cavities, the gas leakage from the cavity is the unknown time function depending on the variable pressure in the cavity $p_c(t)$ and on the gas-leakage type. Determination of the function $\dot{Q}_{out}(t)$ for concrete conditions represents a basic problem of the artificial cavitation theory.

A unified theory of the gas leakage from the ventilated cavity, that allows to calculate the function $\overline{Q}(\sigma)$ for any values of the flow parameters, does not exist. The mechanism of the gas-leakage may be considerably distinguished in dependence on the parameters Fr, σ, σ_v. The gas-leakage rate is also different in the cases of free cavity closure and the cavity closure on a body. Approximate estimations were obtained for some types of the gas-leakage.

1.3 HYDRODYNAMIC SCHEMES OF GAS LEAKAGE FROM THE CAVITY

Observations show that two principally different mechanisms of the gas leakage from the stable artificial cavities exist when the cavity closure is free [2, 3].

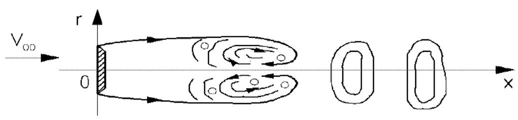

Fig. 3. Scheme of the portion gas-leakage

When magnitudes of the numbers Fr and σ are high, i.e. the gravity effect is not considerable and the cavity shape is close to the axisymmetric one, the cavity tail is filled by a foam which is periodically rejected by portions in the form of toroidal vortices (so called the portion leakage or the first type of gas leakage from the cavity, Fig. 3).

When Fr is fixed and σ is small, i.e. the gravity influence is considerable, the flow in the cavity end becomes well-ordered. The cavity ends by two hollow vortex tubes carrying over the gas from the cavity (so called leakage by vortex tubes or the second type of the gas leakage from the cavity, Fig. 4).

Besides the first and second types of the gas leakage from stable cavities, the third type of the gas leakage exists owing to pulsation of the unsteady ventilated cavities [8, 9].

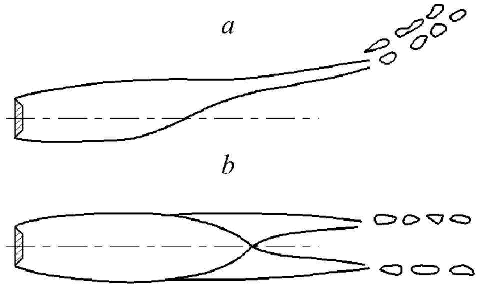

Fig. 4. Scheme of the gas-leakage by vortex tubes: *a* – view from side, *b* – view from above

1.3.1 THE FIRST TYPE (PORTION GAS-LEAKAGE)

The first type of the gas leakage from the artificial cavities is not well studied. This is explained by that in this case the processes at the cavity end are considerably non-stationary and multi-parametric ones. It was shown [3, 10] that they are determined by not only the similarity parameters σ, *Fr* but depend on both the Reynolds number *Re* and the Weber number *We*:

$$Re = \frac{D_n V_\infty}{\nu}, \quad We = \frac{\alpha}{2\rho V_\infty^2 D_n}, \tag{7}$$

where ν is the kinematic coefficient of viscosity; α is the coefficient of water surface tension. They also depend on degree of the free stream turbulence and other external perturbations:

$$\overline{Q} = F(\sigma, \sigma_\upsilon, Fr, \mathrm{Re}, We, \ldots). \tag{8}$$

It was shown experimentally that decrease of numbers *Re* and *We*, i.e. increase of viscosity and surface tension of liquid, causes to decrease of the gas leakage rate from the cavity. Some data and hypothesises about the first type of the gas leakage are presented in the papers by L.A. Epshtein [10, 11].

Qualitatively, in this case processes may be described in the following way. Fluid particles flowing around the axisymmetric cavitator in the radial planes collide in the cavity closure zone and create a non-stationary unstable reentrant jet. When the reentrant jet is distorted, the two-phase medium (foam) is formed. It partially fills the cavity and moves within the cavity in the form of a toroidal vortex. The outer part of this vortex moves along the flow direction under action of viscous shears on the cavity boundary. Its central part moves opposite to the stream under action of the pressure gradient. The vortex continuously grows owing to new foam portions. The foam rejection occurs in the form of a ring toroidal vortex or its part, or separate foam portions (see Fig. 3), when the friction forces become equal to the reentrant motion momentum. Also, the continuous foam leakage from the zone past the rear stagnation point exists simultaneously with the portion leakage.

In the work [10] was shown using the methods of the similarity theory that the expression for a dimensionless period of the foam portions rejection should be in the form:

$$\overline{T} = \frac{V_\infty T}{D_n} = \frac{c_x}{\varsigma}\left(\frac{B_1}{\sqrt{\sigma}} + B_2\right), \tag{9}$$

where c_x is the cavitation drag coefficient, ς is the friction coefficient, B_1, B_2 are the function of *Re, We*.

It follows from the experimental data [12] that an evaluation of Strouhal number Sh for this process is :

$$Sh = \frac{f\,L_m}{V_\infty} \approx 0.315\,,$$

where L_m is the average cavity length. The real process frequency f has values $10 \div 100$ Hz for various tests. It is possible to observe the portion gas-leakage with a stroboscope or using photography with the short exposure time 10^{-4} - 10^{-5} sec.

In the case of the flow close to the natural vapor cavitation when the gravity effect is insignificant, G.V.Logvinovich established the semi-empirical law of the gas-leakage [2]:

$$\dot{Q} = \gamma V_\infty S_c \left(\frac{\sigma_\upsilon}{\sigma} - 1 \right), \tag{10}$$

where $\gamma = 0.01 \div 0.02$ is the empirical constant, S_c is the area of the cavity mid-section.

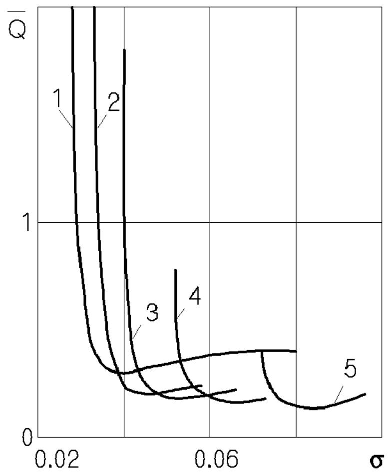

Fig. 5. Influence of the Froude number on $\overline{Q}(\sigma)$:

1 - Fr = 19.3; 2 - 16.5; 3 - 14.6; 4 - 12.7; 5 - 11.0

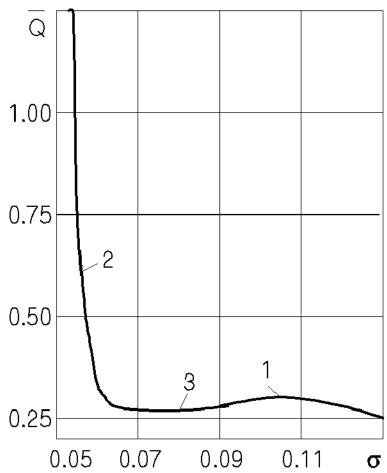

Fig. 6. Experimental dependence $\overline{Q}(\sigma)$

Fr = 13.3

The portion type of the gas-leakage with the periodically arising and distorting reentrant jet is characteristic also in the case of supercavitation flow around hydrofoils with great aspect ratio [6].

1.3.2 THE SECOND TYPE (GAS-LEAKAGE BY VORTEX TUBES)

When the second type of the gas leakage from the artificial cavity, the process is stationary and completely determined by the gravity effect on the cavity. The second leakage type is the most studied both theoretically and experimentally. As is shown in [3, 4], in this case the viscosity and capillarity forces are not considerable. Therefore, from point of view of the similarity theory the dimensionless coefficient of the gas-supply rate into the cavity $\overline{Q}$ must be determined by the dependence:

$$\overline{Q} = F(\sigma\,, Fr). \tag{11}$$

The calculation method of $\overline{Q}$ for the second type of the gas-leakage was proposed for the first time by R.N.Cox and W.A.Clayden [13].

Now the semi-empirical formula by L.A.Epshtein [3] is supposed the most reliable:

$$\overline{Q} = \frac{0.42c_{x0}^2}{\sigma\left(\sigma^3 Fr^4 - 2.5c_{x0}\right)}. \tag{12}$$

Here, c_{x0} is the coefficient of the cavitator drag when σ = 0:

$$c_{x0} = \frac{2F_{x0}}{\rho V_\infty^2 S_n}, \tag{13}$$

where F_x is the cavitation drag; $S_n = \pi D_n^2 / 4$ is the cavitator area. For the disk cavitator $c_{x0} = 0.82$. Also, the more exact semi-empirical formulae were obtained taking into account the cavitator immersion depth H

and density of the gas supplied into the cavity ρ_g, for example [6]:

$$\overline{Q} = \frac{0.271\sqrt{\frac{\rho}{\rho_g}}\, c_{x0}^{2.75} \sqrt{2 - \frac{\sigma Fr^2}{\overline{H}}}}{(Fr - 1.35)\sigma^{1.75} Fr^2 \left(\sigma^3 Fr^4 - 2.38c_{x0}\right)^{1.25}}, \tag{14}$$

where $\overline{H} = H / D_n$. Computations by the formula (14) give satisfactory coincidence with experimental data when $Fr = 4.8 \div 20$.

The experimental dependencies $\overline{Q}(\sigma, Fr)$ showing the influence of Froude number on the gas leakage by vortex tubes are presented in Fig.5 [3].

The gas-leakage type by vortex tubes is characteristic also for the case of supercavitation flow around hydrofoils with small aspect ratio.

A criterion of transition from the first type of the gas leakage to second type is given by the empirical Campbell-Hilborne's criterion [14]:

$$\sigma\, Fr \approx 1; \quad Fr = 5 \div 25\,. \tag{15}$$

Values of $\sigma\, Fr > 1$ correspond to the first (portion) type of the gas-leakage, values $\sigma\, Fr < 1$ correspond to the second type of the leakage (by vortex tubes). As the experiments show, both the mechanisms of the gas leakage from the cavity can act at range of intermediate values of $\sigma\, Fr \approx 1$. Such transient regimes of the gas leakage are very unstable.

A typical experimental dependence of the gas rate coefficient $\overline{Q}$ on the cavitation number σ obtained at testing a series of cones with angles from 30° to 180° (disk) is shown in Fig. 6 [3]. In this case the value of the Froude number was Fr = 13.3. In the expressions for Fr and $\overline{Q}$, so called "universal linear dimension" $D_1 = D_n\sqrt{c_{x0}}$ was used instead D_n to analyze the experimental data. As a result, the relation (11) does not depend on c_{x0}, and all the experimental points for various cones lie on the only curve.

The right part of the graph 1 corresponds to the first portion type of the gas leakage, the left part of the graph 2 corresponds to the second type of the leakage by vortex tubes, the middle part of the graph 3 corresponds to the transient regime. The value σ = 0.081 corresponds to a boundary between the types (15) in this graph.

1.3.3 THE THIRD TYPE (GAS-LEAKAGE FROM PULSATING SUPERCAVITIES)

Denominator in the formula (13) must not be equal to zero. It follows from here that it is impossible to obtain the cavitation number lower than some minimal value at any increase of the gas-supply rate into the cavity:

$$\sigma_{\min} \approx 1.34 \sqrt[3]{\frac{c_{x0}}{Fr^4}} . \tag{16}$$

In practice, when the gas rates are very great, the cavity stability is lost and cardinal change of the mechanism of the gas leakage from the cavity occurs [8, 9].

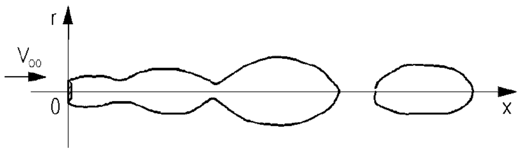

Fig. 7. Scheme of the gas-leakage from the pulsating cavity

Theory of linear stability of the gas-filled axially symmetric cavities was developed by E.V.Paryshev [15]. Analysis showed that the dynamic properties of gas-filled supercavities are mainly determined by the dimensionless parameter

$$\beta = \frac{\sigma_v}{\sigma} . \tag{17}$$

The cavity has a series of fundamental reduced frequencies

$$k = \frac{\omega L_c}{V_\infty} = 2\pi n \qquad n = 1, 2, \ldots , \tag{18}$$

where ω is the circular oscillation frequency; L_c is the cavity length. The following value of the parameter β corresponds to each fundamental frequency

$$\beta_n = 1 + \frac{(\pi n)^2}{6} . \tag{19}$$

Supercavities are stable when $1 \le \beta < \beta_1 = 2.645$ and unstable when $\beta > 2.645$.

Thus, the similarity parameter $\beta \ge 1$, that is equal to ratio of vapor cavition number at given velocity and its real value, is the basic similarity parameter for cavitation flows together with the cavitation number (1) and the Froude number (3). The value $\beta = 1$ corresponds to the natural vapor supercavitation. When the parameter β increases, significance of elasticity of the gas filling the artificial cavity increases as well.

The separated self-induced oscillations of the cavity are established as a result of the stability loss when the supply is permanent. In this case the gas-supply occurs owing to periodic separation of great portions of the cavity (air pockets) (see Fig. 7).

The instability phenomenon and arising the self-induced oscillations take place both for 3-D (in particular, axially symmetric) and for 2-D ventilated cavities. In the work [16], a simple "kinematic" theory of gas-leakage from pulsating cavities was proposed. It gives satisfactory correspondence to the experiment.

1.3.4 GAS-LEAKAGE WHEN THE CAVITY CLOSES ON A BODY

The mechanism of gas leakage from the cavity when the cavity closes on a body is very complicate and depends on number of factors such as:

a) **cavity perturbations**: its floating-up, wave deformations, natural distortion of the free boundary;

b) **body parameters**: shape in the closure place, surface roughness, vibrations;

c) **closure conditions**: angle of free boundary inflow, presence of the liquid and gas jets, radial velocity at the closure place.

According to the known theoretical schemes of the supercavity closure [17] the cavity may close on a solid body in the following ways (see Fig. 8):

a) **Riabouchinsky scheme**. The cavity smoothly closes on a solid surface–closurer located in the cavity end. In the closure place, the body diameter is $D_b < D_c$.

b) **Joukowski–Roshko scheme**. The cavity closes on a cylinder with diameter equal to the diameter of the biggest cavity section D_c.

c) **Gilbarg–Efros scheme**. The cavity closes on a cylinder with diameter $D_b < D_c$ with forming the ring reentrant jet.

The experience of work with the artificial cavity shows that the gas leakage may be compared with the rate of fluid supplied into the cavity with the reentrant jet. Physically, this may be explained that the fluid inflowing into the cavity aerates, mixes with the gas and rejects from the cavity as a mixture of gas and water.

Using the momentum conservation equation, the cross section area of the reentrant jet when the cavity closure is free is equal [7]:

$$S_j = \frac{c_x}{4}\frac{\pi D_n^2}{4}. \tag{20}$$

In the case of the cavity closure on the body, the section area of the ring reentrant jet remains the same. It was established experimentally that when the cavity closes on a circular cylinder with diameter D_b, the gas leakage is proportional to a ratio of section areas of the middle cavity part $\pi D_c^2/4$ and one of the cylinder $\pi D_b^2/4$:

$$\dot{Q} = k_2 V_\infty S_j \left(1 - \frac{D_b^2}{D_c^2}\right), \quad D_b \le D_c, \tag{21}$$

where k_2 is some empirical coefficient. When $D_b = 0$, we have free closure of the cavity by the first type of the gas-leakage. When $D_b = D_c$, we obtain the cavity closure by the Joukowski–Roshko scheme with the zero gas leakage (see Fig. 8, b).

Theoretically, we can also obtain the zero gas leakage when the cavity closes on the body by the Riabouchinsky scheme (see Fig. 8, a) when $D_b < D_c$, if the cavity and body curvatures are coordinated at the closure point $\alpha = \alpha_b$ (Fig. 9).

Practically, it is impossible to obtain the zero gas leakage at high magnitudes of *We* and *Re* numbers. However, it may be reduced to the minimal value caused by presence of unremovable small-scale perturbations. Blowing or suction of fluid is applied at the closure place to realize the stable cavity closure [18]. For example, the works [18, 19] propose a scheme of stable closure of the cavity on the liquid jet outflowing from the slot in the closurer of the elliptic shape.

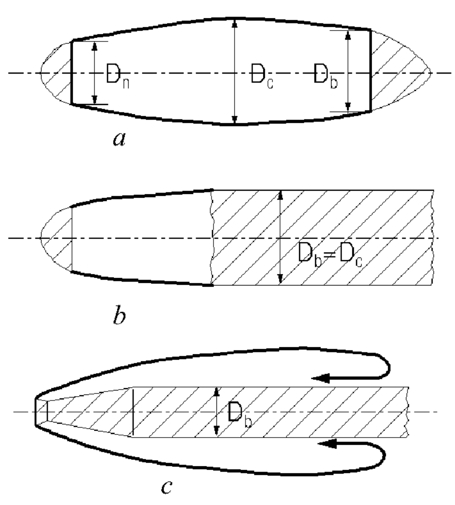

Fig. 8. Schemes of the supercavity closure on a body: *a* – Riabouchinsky; *b* – Joukowski-Roshko; *c* – Efros-Gilbarg

We have discovered experimentally the interesting phenomenon of hysteresis at the control of the ventilated cavity closing on the body by regulating the gas-supply. This effect increases with increasing the body surface curvature.

The control of ventilated cavity is possible, if single-valued dependence of the cavity length on the gas supply rate exists: $L_c = L_c(\dot{Q})$. If we consider neighborhood of the point of the cavity closure on rectilinear generatrix of the body $y = y_b$ (Fig. 10), we can note that the closure angle α will be increased with increasing the cavity dimensions:

$$\alpha(L_1) < \alpha(L_2) < \alpha(L_3), \qquad L_1 < L_2 < L_3$$

due to increasing both the ratio D_c / y_b and the relative cavity dimensions. In this case the velocity on the cavity boundary changes insignificantly due to the cavitation number varies weakly. Thus, the gas-leakage value $\dot{Q}$ depends mainly on the local angle of the cavity closure on the body:

$$\dot{Q} \approx \dot{Q}(\alpha).$$

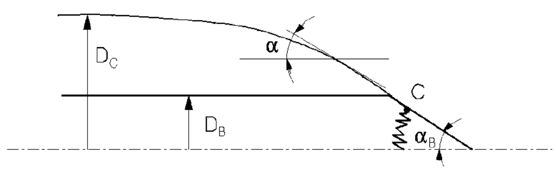

Fig. 9. Scheme of the fluent cavity closure on a body

Dependence of the gas-leakage on the cavity length $\dot{Q}_1(L_c)$ is schematically shown by dotted line in Fig. 10 when the cavity closes on the rectilinear generatrix of the body $y = y_b$.

Qualitatively, appearance of hysteresis behaviour may be explained by locating an additional triangle-shaped body on the rectilinear generatrix (it is dashed in Fig. 10). The cavity length increases with increasing the gas-supply from the value $\dot{Q}_1$. When the cavity closes on the frontal surface of the triangle

$x_1 \div x_2$, the cavity forms bigger angles of closure than at closure on the rectilinear generatrix. For example, $\alpha(x_2)$ is bigger than ones when the cavity closes between the points x_1 and x_4. We have $\alpha(x_2) = \alpha(x_4)$ only in the point x_4. Therefore, the gas rate $\dot{Q}_2$ for maintenance of the cavity closing in the point x_2 will exceed rates when the cavity closes in the points $x_2 \div x_4$ and equal to the rate for maintenance of the cavity closing in the point x_4. As a result, the cavity length will very rapidly increase from $L_c = L_2$ to $L_c = L_4$.

With decreasing the supply from the value $\dot{Q}_2$, when the cavity closure point is on the back side of the triangle $x_2 \div x_3$, the closure angle will be smaller than one when the cavity closes on the rectilinear generatrix. When the cavity closes in the point x_2, the rate $\dot{Q}_1$ will be smaller than one when it closes between the points x_1 and x_2. As a result, the cavity length will decrease very rapidly from the value $L_c = L_2$ to the value $L_c < L_1$.

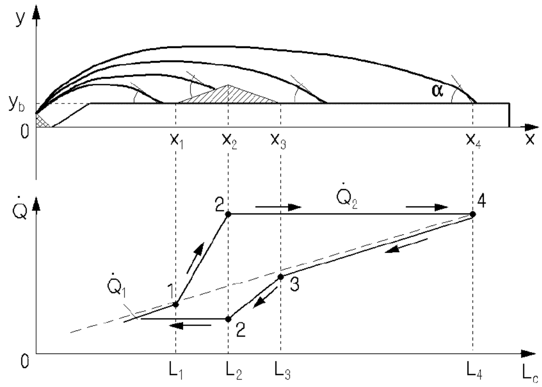

Fig. 10. Scheme of a hysteresis when the cavity closes on a body

Thus, a hysteresis loop appears in the graph $\dot{Q}(L_c)$ that is formed when the gas supply into the cavity increases or decreases.

The hysteresis property of the function of the gas supply into the ventilated cavity may by practically used to stabilize the cavity closure on the body by respective designing the body shape.

2 Approximate calculation of the steady axisymmetric supercavity

As it is known, main properties of supercavitation flows are well described by the potential theory of ideal incompresssible fluid. The respective mathematical problems are related to the class of mixed boundary value problems for harmonic functions. The flow area is bounded by the solid and free boundaries. The velocity distribution is given on the solid boundaries (cavitator or hydrofoil), the constant pressure p_c is given on the unknown free boundaries. For stationary problems, the velocity constancy along the free boundaries follows from the pressure constancy:

$$V_c = V_\infty \sqrt{1+\sigma} = const\,. \tag{22}$$

In this case the free boundaries are lines of flow.

Potential models of developed cavitation flows do not describe a real flow in the cavity closure zone where capillarity and viscosity are considerable. According to the known Brilluene paradox, existence of a closed cavity in the imponderable flow is impossible [1]. This resulted in creation of a number of schemes of "mathematical" closure of the supercavity: by Riabouchinsky, Joukowski-Roshko, Efros-Gilbarg et al [17].

2.1 FORMULATION OF PROBLEM

We consider steady axially symmetric flow around a supercavitating disk in unbounded imponderable fluid with the velocity at infinity V_∞. We introduce the cylindrical coordinate system *Oxr* connected with the cavitator (Fig. 11). Let $r = R(x)$ is the equation of the cavity generatrix.

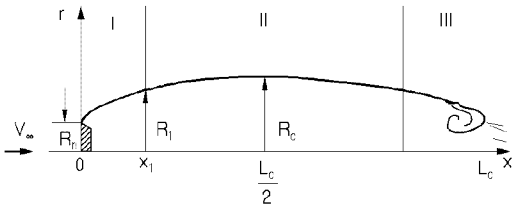

Fig. 11. Scheme of an axisymmetrical supercavity

The Laplace equation for the perturbed velocity potential $\varphi(x,r)$ is valid for all the flow area:

$$\frac{\partial^2\varphi}{\partial x^2}+\frac{\partial\varphi}{\partial r^2}+\frac{1}{r}\frac{\partial\varphi}{\partial r}=0. \qquad (23)$$

On the cavity surface, the potential φ must satisfy both the boundary condition of zero normal velocity (the kinematic boundary condition)

$$\frac{\partial\varphi}{\partial r}=\left(V_\infty+\frac{\partial\varphi}{\partial x}\right)\frac{dR}{dx}, \qquad r=R(x) \qquad (24)$$

and the cavity pressure to be constant $p = p_c$ (the dynamic boundary condition). Applying the Bernoulli equation on the liquid contour, we can write the dynamic boundary condition in the form:

$$\left(\frac{\partial\varphi}{\partial r}\right)^2+\left(\frac{\partial\varphi}{\partial x}\right)^2+2V_\infty\frac{\partial\varphi}{\partial x}=\frac{2\Delta p}{\rho}, \quad r=R(x)\,, \qquad (25)$$

where $\Delta p = p_\infty - p_c$. The third condition is the condition of the perturbations to be vanished at infinity

$$\varphi\to 0, \qquad x^2+r^2\to\infty \qquad (26)$$

Owing to great mathematical difficulties an exact solution of the boundary value problem (23)-(26) has been not obtained. In contrast to two-dimensional problems on supercavitation flows, it is impossible to apply the power mathematical theory of analytical functions and conformal mapping in this case. Some progress of applying the theory of generalized analytical functions to axisymmetric problems was outlined last years [20].

All known results of the theory of axisymmetric cavities have been obtained by numerical methods or by approximate asymptotic and semi-empirical methods and perturbation method as well.

P.Garabedian's works [21] are very important and imperishable for the theory of axisymmetric super-cavitation flows. He sought a solution of the axisymmetric problem for stream-function $\psi(x,r)$ and consider it as the plane flow perturbation. As a result, he obtained the asymptotic solution for main dimensions of the supercavity past a disk when $\sigma \to 0$:

$$D_c = D_n\sqrt{\frac{c_x}{\sigma}},\quad L_c = D_n\frac{A\sqrt{c_x}}{\sigma},\quad A=\sqrt{\ln\frac{1}{\sigma}},\quad c_x(\sigma)=c_x(0)(1+\sigma),\quad c_x(0)=0.827, \tag{27}$$

where D_n is the disk diameter; D_c is the biggest cavity section diameter; L_c is the cavity length.

A comparison of the asymptotic formulae (27) with both the experimental data and the "exact" numerical calculations showed their high precision and physical accuracy.

2.2 APPROXIMATION RELATIONS

A combined approach using reliable physical representations, general conservation laws (such as the momentum and energy theorems) and generalized experimental data proved to be the historically first and most productive in practical calculations. G.V. Logvi-novich was a founder of this direction of the super-cavitation flow investigation.

We present firstly some useful relations for the axisymmetric supercavities obtained by approximating both the experimental data and the "exact" numerical calculations

For main dimensions of the axisymmetric cavity (the mid-section diameter D_c and the cavity length L_c) in the case of the cavitation number is small and the gravity influence is negligible, it was obtained semi-empirical relations of the same structure as in (27) [2, 3]:

$$D_c = D_n\sqrt{\frac{c_x}{k\sigma}},\qquad L_c = D_n\frac{A\sqrt{c_x}}{\sigma}, \tag{28}$$

where $k = 0.9 \div 1.0$, A are empirical constants. When σ is not very small, it is usually accepted $A \approx 2$.

Formulae (28) are valid not only for the disk but for any blunted cavitators. For a non-disk cavitator D_n is a diameter of the cavity separation line. For the drag coefficient of the blunted cavitators when σ is sufficient small, the approximate Reichardt formula is valid [1-4]:

$$c_x(\sigma) = c_{x0}(1+\sigma),\qquad 0<\sigma<1.2, \tag{29}$$

where c_{x0} is the cavitator drag coefficient when $\sigma = 0$. Value $c_{x0} \approx 0.82$ was established experimentally for the disk cavitator. For cavitators in the form of a blunted cone with cone angle $120° \le \beta \le 180°$, it is possible to use the formula:

$$c_{x0} = 0.13 + \sqrt{0.0036\beta - 0.1719}, \tag{30}$$

that was obtained by approximating the experimental data for the disk and cones [3].

Analysis of photographs of supercavities past the blunted cavitators when σ is small permits to distinguish three characteristic parts of the cavity (Fig. 11). The frontal part I adjoining to the cavitator has length of order of D_n. It is characterized by strong curvature of the free boundary. The next main part II occupies approximately ¾ of the cavity length L_c. Finally, the tail part III has unstable unsteady boundaries at the moderate magnitudes of σ. It is impossible to determine them using the potential theory.

The frontal part boundaries have great curvature and are determined by the cavitator shape. They do not depend on the cavitation number. For the disk cavitator, the empirical "1/3 law" is usually used [2]:

$$\frac{R}{R_n} = \left(1 + \frac{3x}{R_n}\right)^{\frac{1}{3}}, \qquad \frac{x}{R_n} < 3 \div 5, \tag{31}$$

where $R(x)$ is the current cavity radius, $R_n = D_n / 2$ is the disk radius.

The IHM of Ukrainian NAS accumulated great experimental material on the free motion of supercavitating models with the disk cavitators in wide range of velocities $V = 50 \div 1400$ m/sec. The corresponding cavitation numbers are $\sigma = 1.4 \cdot 10^{4} \div 10^{2}$. Natural vapor cavities are formed for all the pointed velocity range. They are axially symmetric along the whole their length, i.e. are not deformed under the gravity effect.

For the main supercavity part past the disk, we obtained the semi-empirical formula [22]:

$$\overline{R}^2 = 3.659 + 0.847(\overline{x} - 2.0) - 0.236\sigma(\overline{x} - 2.0)^2, \qquad \overline{x} \ge 2.0 \tag{32}$$

where $\overline{R} = R / R_n$, $\overline{x} = x / R_n$. In this case, the experimental data was used which were obtained for natural vapor supercavities in range of the cavitation number $\sigma = 0.012 \div 0.057$. Results of measuring the profile of the steady vapor cavities corresponding to various values of σ are presented in Fig. 12. Fig. 13 presents a photograph of the vapor supercavity closing on the jet out-flowing from the model nozzle. The frontal cavity part at $\overline{x} < 2.0$ is described by formula (31).

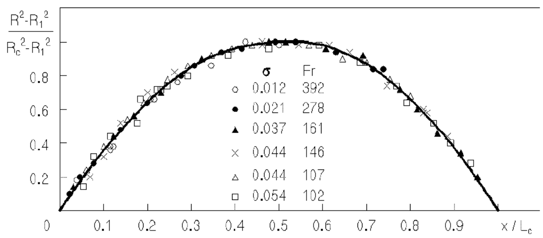

Fig. 12. Universal contour of the axisymmetrical supercavity

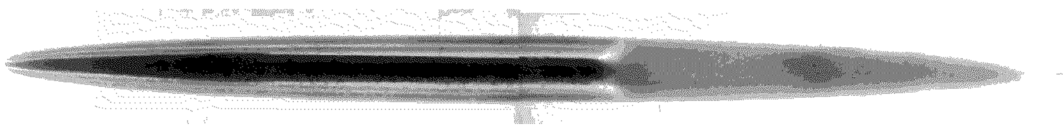

Fig. 13. View of the natural vapor supercavity past the disk: D_n = 15 mm, V = 105 m/sec, σ = 0.0204.

From the formula (32) one has the following expressions for both the cavity mid-section radius and the cavity length:

$$\overline{R}_c = \frac{R_c}{R_n} = \sqrt{3.659 + \frac{0.761}{\sigma}}, \tag{33}$$

$$\overline{L}_c = \frac{L_c}{R_n} = 4.0 + \frac{3.595}{\sigma}. \tag{34}$$

The functions $\overline{R}_c(\sigma)$ and $\overline{L}_c(\sigma)$ which are calculated by formulae (33), (34) in range of cavitation number $\sigma = 0.01 \div 0.06$ are shown by solid lines in Fig. 14. The experimental data of Fig. 12 also are plotted there. For comparison, the same functions given by asymptotic formulae by P.Garabedian (27) are plotted by dotted lines.

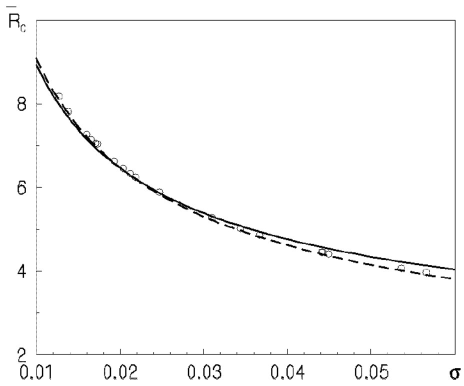

a

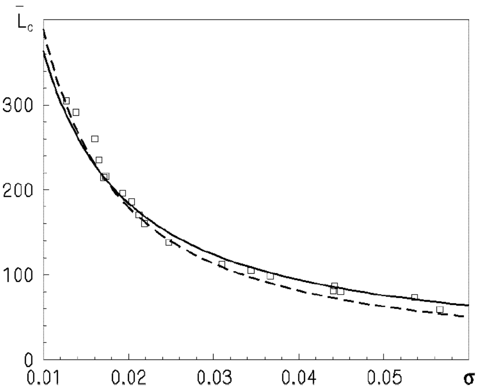

b

Fig. 14. Approximate dependencies $\overline{R}_c(\sigma)$ (a) and $\overline{L}_c(\sigma)$ (b) calculated by formulae (33) and (34)

An advantage of approximation formula (32) is that it gives explicit dependence of the cavity shape on the cavitation number.

We also present other approximation formulae for the main dimensions of stationary axisymmetric super-cavities past cones and the cavitation drag coefficient of cones. They were obtained based on the numerical calculations in "exact formulation" [23, 24]:

$$\frac{D_c}{D_n} = \sqrt{\frac{c_x}{\kappa\sigma}}, \qquad \kappa = \frac{1+50\sigma}{1+56.2\sigma}, \qquad \frac{L_c}{D_n} = \left[\frac{1.1}{\sigma} - \frac{4(1-2\alpha)}{1+144\alpha^2}\right]\sqrt{c_x \ln\frac{1}{\sigma}}, \tag{35}$$

where D_n is the cone base diameter.

$$c_x = c_{x0} + (0.524 + 0.672\alpha)\sigma, \qquad 0 \le \sigma \le 0.25, \qquad \frac{1}{12} \le \alpha \le \frac{1}{2}, \tag{36}$$

$$c_{x0} = 0.5 + 1.81(\alpha - 0.25) - 2(\alpha - 0.25)^2, \quad \frac{1}{12} \le \alpha \le \frac{1}{2}, \qquad c_{x0} = \alpha(0.915 + 9.5\alpha), \qquad 0 < \alpha < \frac{1}{2},$$

where $\alpha\pi$ is the cone half-angle. When $\sigma \to 0$, the formulae (35), (36) transform into the asymptotic relations by P.Garabedian (27).

2.3 ENERGY APPROACH

According to G.V.Logvinovich work [2] we use the theorem of momentum to obtain the approximate equation for the main supercavity part. We display the check volume of liquid (Fig. 15). It has such boundaries:

S_1 is a plane perpendicular to the symmetry axis and located far up-stream ;

S_2 is a plane perpendicular to the symmetry axis and passed through an arbitrary point of the cavity axis before the biggest cavity section;

S_3 is a cylindrical surface with the axis coinciding with the cavity symmetry axis and with radius $R_2 \to \infty$. Let $R(x)$ is the radius of the cavity section by the plane S_2, so that $S = \pi R^2$ is the cross-

section area. We write the theorem of momentum for the displayed fluid volume in projection on the x-axis:

$$\int_{S_2-S} \rho(V_\infty + v_x)^2 ds - \int_{S_1} \rho V_\infty^2 ds = \int_{S_1} p_\infty^2 ds - \int_{S_2-S} p ds - Sp_c - F_x, \quad (37)$$

where F_x is the cavitation drag. Integrals with respect to the cylindrical surface S_3 vanish, since the perturbed velocity reduces as $1/r^3$ when $r \to \infty$ (like a flow of a dipole).

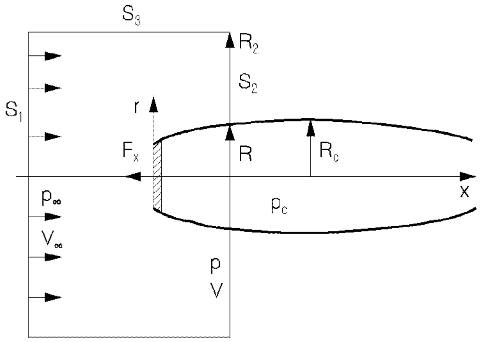

Fig. 15. Scheme of application of the theorem of momentum

From the Bernoulli equation, we obtain the pressure:

$$p = p_\infty - \rho V_\infty v_x - \frac{1}{2}\rho v_r^2, \quad (38)$$

and use condition of conservation of the mass of fluid flowing through the sections S_1 and $S_2 - S$:

$$\int_{S_1} \rho V_\infty^2 ds = \int_{S_2-S} \rho(V_\infty + v_x)^2 ds.$$

It follows from this that

$$\int_{S_2-S} v_x ds = V_\infty S. \quad (39)$$

Substituting (38) and (39) in the Eq. (37), we obtain the relation for cavitation drag:

$$F_x = \Delta p S - \int_{S_2-S} \frac{\rho v_x^2}{2} dx + \int_{S_2-S} \frac{\rho v_r^2}{2} ds, \quad (40)$$

where $\Delta p = p_\infty - p_c$.

If, in particular, we draw the plane S_2 through the cavity mid-section, then $S = S_c$ and $v_r = 0$. Hence, the second integral in the Eq. (40) is strictly equal to zero. It is possible to show that the first integral in the Eq. (40) is small compared to the first term when $\sigma \to 0$ [2]. That is why, we also cast it out introducing a correcting multiplier k. After that, the law of the supercavitation drag may be written in the form:

$$F_x = k\Delta p S_c = k\sigma S_c \frac{\rho V_\infty^2}{2}. \quad (41)$$

Introducing the cavitation drag coefficient of the cavitator (13) in the Eq. (41), we obtain the formula (28) for the supercavity mid-section radius:

$$R_c = R_n \sqrt{\frac{c_x}{k\sigma}}\,.$$

Experimental check and comparison with numerical calculations showed that the correcting multiplier k weakly depends on σ and has magnitude in range 0.9 ÷ 1.0. It is usually accepted $k = 1$ for practical calculations.

Then, we transform the Eq. (40) to the differential equation of the supercavity section expansion. Neglecting the first integral in the Eq. (40), we may consider the flow in the plane S_2 as pure radial one. We have the boundary condition for the mean part of the slender supercavity surface

$$v_x \approx V_\infty R'(x). \tag{42}$$

The radial velocity of fluid at the arbitrary radius r is determined from the condition of the mass conservation:

$$2\pi R\, v_r(R) = 2\pi\, r v_r(r),$$

then we obtain taking into account the Eq. (42):

$$v_r(r) = V_\infty \frac{RR'}{r}\,. \tag{43}$$

The integral in the Eq. (40) represents the kinetic energy of the flow in the fluid layer E_k. It is equal to

$$E_k = \int\limits_{S_2 - S} \frac{\rho v_r^2}{2} ds = \pi\rho V_\infty (RR')^2 \ln r \Big|_{r=R}^{r=\infty}. \tag{44}$$

One can see that this integral value is equal to infinity, i.e. infinite energy is necessary for the radial expansion of the cavity in the two-dimensional problem. That is why we accept two non-strict but plausible assumptions:

1) Let, according to [1], the outer radius of the flow area R_2 has high but finite magnitude. In other words, we suppose that all perturbations of the fluid motion are concentrated in a ring with the inner radius R and the outer radius R_2. This supposition is plausible, because the velocity perturbation decay very rapidly (as $1/r^3$) in the three-dimensional problem.

2) Let the logarithm magnitude

$$\mu = \ln \frac{R_2(x)}{R(x)} \tag{45}$$

does not depend on the coordinate x. This assumption is plausible for the mean part of the slender cavity when $\sigma \to 0$.

Then the relation (40) may be rewritten in the form

$$F_x = \Delta p S + \frac{\mu}{4\pi} \rho V_\infty^2 (S')^2. \tag{46}$$

Differentiating the Eq. (46) with respect to S, we obtain another form of the equation of the supercavity section expansion that does not contain the cavitation drag:

$$\mu \frac{\partial^2 S}{\partial x^2} = -\frac{2\pi \Delta p}{\rho V_\infty^2}\,. \tag{47}$$

Passing to the fixed coordinate system in the Eq. (47) with the independent variable substitution $x = V_\infty t$, we rewrite it in the form

$$\mu \frac{\partial^2 S(\tau,t)}{\partial t^2} = -\frac{2\pi \Delta p}{\rho}. \tag{48}$$

The Eq. (48) assumes the obvious mechanical explanation:

The cavitator passes the fixed "observation plane" at the time $t = \tau$ and makes an orifice with diameter D_n in that plane. Considerable radial velocities arise on that orifice boundaries. Then, that orifice expands on inertia overcoming the pressure difference Δp up to its maximal diameter D_c at the time $t = \tau + t_c$. After that, the orifice decreases and closes again at the time $t = \tau + 2t_c$.

The time interval $t_c = L_c / 2V_\infty$ is called "the time of the complete cavity expansion". After the cavity collapse, the wake remains past it where the mechanical energy transmitted by the cavitator to the fluid disperses into heat.

The Eq. (48) allows to calculate an expansion of each cavity section separately, i.e. it is an expression of the independence principle for expansion of the slender axisymmetric cavity sections by G.V.Logvinovich [2].

A full cavity profile at fixed *t* may be calculated when $t - 2t_c \le r \le t$. In this case x-coordinates of the cavity sections are $x(\tau) = V_\infty \tau$, and the cavity length is equal to $L_c = 2t_c V_\infty$.

The more strict analysis of the Eq. (40) [2] permits to transform it to the following form (in the fixed coordinate system):

$$\frac{\kappa}{2}(t - t_c)\frac{\partial S}{\partial t} + (S_c - S) = 0, \tag{49}$$

where κ is some correcting coefficient. The integral of the Eq. (49) is

$$S(t) = S_c + C(t - t_c)^{2/\kappa}.$$

Determining the arbitrary constant *C* from the initial condition $S(0) = S_n$, we finally obtain the law of the cavity section expansion:

$$S(t) = S_c\left[1 - \left(1 - \frac{S_n}{S_c}\right)\left(1 - \frac{t}{t_c}\right)^{2/\kappa}\right]. \tag{50}$$

Passing in the Eq. (50) to the coordinate system related with the cavitator $x = V_\infty t$, we obtain:

$$R(x) = R_c\sqrt{1 - \left(1 - \frac{R_n^2}{R_c^2}\right)\left(1 - \frac{2x}{L_c}\right)^{2/\kappa}}. \tag{51}$$

For non-disk cavitators, the coordinate $x = 0$ corresponds to the plane of the cavity separation.

A comparison with experiments showed that value of the correcting coefficient is $\kappa \approx 0.85$. However, the exact enough results are obtained when $\kappa = 1$.

It is easy to see that the shape of the main part of the axisymmetric supercavity represents an ellipsoid of revolution when $\kappa = 1$, and one is very close to it when $\kappa = 0.85$.

Experience of calculation shows that the expressions (31), (51) must be "matched" on the boundary between the frontal and the main cavity parts when $x = x_1 \approx D_n$. As a result, we obtain so called formula of the G.V.Logvinovich's composed cavity:

$$R(x) = R_n\left(1 + \frac{3x}{R_n}\right)^{\frac{1}{3}}, \qquad x \le x_1, \qquad R(x) = R_c\sqrt{1 - \left(1 - \frac{R_1^2}{R_c^2}\right)\left(1 - 2\frac{x - x_1}{L_c - 2x_1}\right)^{2/\kappa}}, \tag{52}$$

where $R_1 = R(x_1)$ is the "agreement section" radius. When $x_1 = D_n$, we just obtain from the Eq. (31) that $R_1 = 1.913$.

The "universal contour" of the ellipsoidal cavity is plotted by solid line in the Fig. 12. It was calculated by the formula (52) when $\kappa = 1$. A comparison with the experimental data shows good coincidence along the whole cavity length right up to the point of the cavity closure on the body.

2.4 ASYMPTOTIC APPROACH

Great aspect ratio of supercavities when σ is small gives background to apply the theory of flow around slender bodies [25, 26] to calculate them. Basing on this theory, the asymptotic theory of a slender axisymmetric cavity was developed [27-30]. The basic mathematical tool of this theory is asymptotic method of singular perturbations [26]. A solution of the axisymmetric boundary value problem is sought in the form of decomposition by the small parameter ε. Its value is inverse to the cavity aspect ratio.

It is well known from the theory of slender bodies that the potential decomposition near the x-axis is [26]:

$$\varphi = \frac{V_\infty}{2}\frac{dR^2}{dx}\ln r + \ldots$$

To evaluate the order of smallness of terms in the Eqs. (23)-(25), we substitute there orders of smallness for all the variables:

$$r \sim \varepsilon, \quad R \sim \varepsilon, \quad x \sim 1, \quad \varphi \sim \varepsilon^2 \ln\varepsilon, \quad \Delta p \sim \varepsilon.$$

As a result, neglecting the terms of high order of smallness, we come to the "internal" problem of the first approximation:

$$\frac{\partial^2\varphi}{\partial r^2} + \frac{1}{r}\frac{\partial\varphi}{\partial r} = 0, \tag{53}$$

$$\frac{\partial\varphi}{\partial r} = V_\infty\frac{dR}{dx}, \qquad when \quad r = R(x), \tag{54}$$

$$V_\infty\frac{\partial\varphi}{\partial x} = \frac{\Delta p}{\rho}, \qquad when \quad r = R(x). \tag{55}$$

We note that the condition (26) proves to be lost in the internal problem.

We verify by direct substitution that the general solution of the Eq. (53) satisfying to the kinematic condition (54) is:

$$\varphi(x) = \frac{V_\infty}{2}\frac{dR^2}{dx}\ln r + C(x), \tag{56}$$

where $C(x)$ is some arbitrary function that may be determined by matching with the "external" solution satisfying to the condition (26) [26].

Substituting the solution (56) to the dynamic boundary condition (55), we obtain the equation:

$$\frac{d^2R^2}{dx^2}\ln R+\frac{2C'(x)}{V_\infty}=\frac{2\Delta p}{\rho V_\infty^2}. \tag{57}$$

We introduce a new arbitrary function $\Psi(x)$ instead $C(x)$ using the equality:

$$C'(x)=-\frac{V_\infty}{2}\frac{d^2R^2}{dx^2}\ln\Psi(x).$$

Then the Eq. (57) becomes the same form as the Eq. (47):

$$\frac{d^2R^2}{dx^2}\ln\frac{R(x)}{\Psi(x)}=\frac{2\Delta p}{\rho V_\infty^2}, \tag{58}$$

if we consider that

$$\ln\frac{\Psi(x)}{R(x)}=\mu=const.$$

Thus, both the energy theory and the asymptotic theory of slender axisymmetric cavities yield the same equation in the first approximation.

The more strict analysis of the boundary value problem (53)-(55) permits to obtain the differential equation

$$\frac{\partial^2R^2}{\partial x^2}\ln\frac{R}{\Psi}+\left(\frac{dR}{dx}\right)^2=\frac{2\Delta p}{\rho V_\infty^2}, \tag{59}$$

having the higher precision $\varepsilon^2\ln\varepsilon$ than the Eq. (58).

In the work [30], its solution was constructed by the method of matched asymptotic decomposition.

However, the equation of the first approximation (48) is the more convenient for practical calculations. It must be integrated when $t>\tau$ with the starting conditions:

$$S(\tau,\tau)=\frac{\pi D_n^2}{4},\qquad \frac{\partial S(\tau,\tau)}{\partial t}=\dot S_0, \tag{60}$$

where $\dot S_0$ is the starting velocity of the cavity section expansion. It is determined by the cavitator shape, i.e. by D_n and c_{x0}, and also by the model velocity V and does not depend on the cavitation number.

The Eq. (48) reminds the Newton equation of motion. The constant μ may have certain physical sense of the additional mass coefficient of the expanding cavity section (so called the ring model of the slender axisymmetric cavity [1, 30]). This assumption allows to determine the starting velocity of the cavity section expansion [29]:

$$\frac{\partial R^2}{\partial t}=2\sqrt{\frac{F_x}{k\pi\mu\rho}},\qquad t=\tau. \tag{61}$$

However, for practical calculations it is rational to determine both the constant μ and the initial velocity of the section expansion $\dot S_0$ in such way that the semi-empirical relations (28) are fulfilled. Integrating twice the Eq. (48), we obtain:

$$\frac{\partial S}{\partial t}=\dot S_0-\frac{k_1\Delta p}{\rho}(t-\tau), \tag{62}$$

$$S=S(\tau,\tau)+\dot S_0(t-\tau)-\frac{k_1\Delta p}{2\rho}(t-\tau)^2, \tag{63}$$

where $k_1 = 2\pi / \mu$. Substituting the expressions (62) and (63) into obvious relations:

$$S(\tau, \tau + t_c) = \frac{\pi D_c^2}{4}, \qquad \frac{\partial S(\tau, \tau + t_c)}{\partial t} = 0,$$

and taking the Eq. (28) into account, we finally obtain:

$$\dot{S}_0 = \frac{k_1 A}{4} D_n V_\infty \sqrt{c_{x0}}, \qquad k_1 = \frac{4\pi}{A^2}. \tag{64}$$

The Eq. (48) is an equation of the ellipsoid of revolution, i.e. it correctly describes the shape of the main cavity part. To take into account the frontal part (31), it is necessary to use the condition $S(\tau, \tau) = \pi D_1^2 / 4$ (here, D_1 is the "agreement section" diameter) instead the first of starting conditions (60).

Fig. 16 gives a comparison of the cavity shape calculated by formulae (52), (63) and (32) when $\sigma = 0.02$.

If $\sigma < 0.01$, all three curves coincide. The cavity contour approaches to the ellipsoidal cavity shape (52) when σ decreases and practically coincides with the latter when $\sigma < 0.01$.

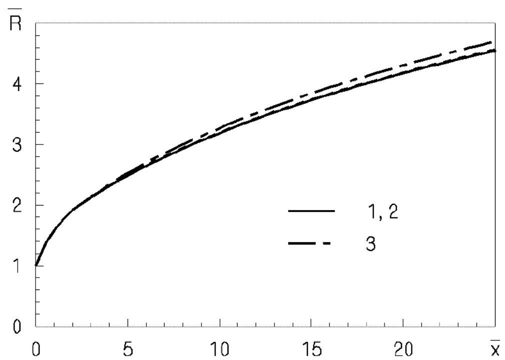

Fig. 16. Supercavity shape calculated by formulae: 1- (32); 2 - (52); 3 - (63)

3 Calculation of unsteady supercavities

3.1 INDEPENDENCE PRINCIPLE OF CAVITY EXPANSION BY G.V. LOGVINOVICH

In 50s G.V.Logvinovich proposed and grounded so named principle of independence of the slender axisymmetric cavity section expansion. It may be treated as a partial case of the general mechanical principle of plane sections. That principle consists in that the law of the cavity section expansion almost does not depend on the previous and the next motion of the cavitator. That law is determined by the instantaneous velocity of the cavitator at passing through this section plane and by the pressure difference $\Delta p = p_\infty - p_c$ as well. The independence principle of the cavity expansion is of very importance to research the unsteady supercavitation flows.

3.2 EQUATION OF AN UNSTEADY SUPERCAVITY

In the case of unsteady axisymmetric cavities the independence principle consists in that the law of arbitrary section expansion about the trajectory of the cavitator center is determined by the cavitator instantaneous velocity at passing this section $V(t)$, and also the pressure difference $\Delta p = p_\infty - p_c$ that can

depend on time at fluctuating the external pressure $p_\infty(t)$ or the cavity pressure $p_c(t)$ as well. The mathematical expression of the independence principle is the equation of expansion of the unsteady cavity section [29]:

$$\frac{\partial^2 S(\tau,t)}{\partial t^2} = -\frac{k_1 \Delta p(\tau,t)}{\rho}, \quad x(t) - L_c(t) \le \xi \le x(t), \tag{65}$$

where $\Delta p(\tau,t) = p_\infty(\xi) + p_1(t) - p_c(t)$. Here, $\tau \le t$ is the time of the section ξ formation; $x(t)$ is the current absolute coordinate of the cavitator (see Fig. 17); $p_1(t)$ is the perturbation of the ambient pressure. The hydrostatic pressure p_∞ can change from a section to section in case of the vertical cavity in ponderable fluid.

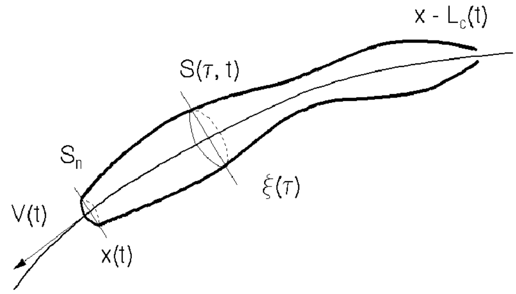

Fig. 17. Calculation scheme of an unsteady supercavity

According to the independence principle, the equations of expansion of the steady cavity (48) and the nonsteady cavity (65) are identical. The constant $k_1 = 2\pi/\mu$ and the initial velocity of the section expansion $\dot{S}(t,t) = \dot{S}_0$ have the same magnitudes (64). In this case $V = V(\tau)$ is the instantaneous cavitator velocity at the time of the section ξ formation.

We introduce the dimensionless variables by formulae:

$$x = D_n x', \quad L_c = D_n L_c', \quad S = D_n^2 S', \quad t = \frac{D_n}{V_\infty} t', \quad p = \rho V_\infty^2 p'.$$

The Eq. (65) for the dimensionless variables is (the primes are omitted):

$$\frac{\partial^2 S(\tau,t)}{\partial t^2} = -k_1 \Delta p(\tau,t) = -\frac{k_1 \sigma(\tau,t)}{2} V^2(\tau), \quad t - L_c(t) \le \tau \le t. \tag{66}$$

The Eq. (66) must be integrated with dimensionless initial conditions:

$$S = \frac{\pi}{4}, \qquad \frac{\partial S}{\partial t} = \frac{k_1 A}{4} V(\tau)\sqrt{c_{x0}}, \qquad t = \tau. \tag{67}$$

The cavitation number is a time function, if the external pressure $p_\infty(t)$ and/or the cavity pressure $p_c(t)$ fluctuate. The cavitator velocity V also is a time function in the general case. For example, in case of the vertical motion of the supercaviating model under action of only cavitation drag the cavitator velocity and the cavitator position are determined by the equations:

$$m\frac{dV}{dt} = -\frac{\rho V_\infty^2}{2} S_n c_{x0}\left[1 + \frac{p_{atm} + \rho g H(t) - p_c(t)}{\rho V_\infty^2/2}\right], \qquad H(t) = \int_0^1 V(s)ds,$$

where m is the body mass; p_{atm} is the atmospheric pressure; H is the cavitator immersion depth.

Twice integrating the Eq. (66) with taking into account the initial conditions (67), we obtain the formula:

$$S(\tau,t)=\frac{\pi}{4}+\frac{k_1V(\tau)}{4}\left[A\sqrt{c_{x0}}\,(t-\tau)-2V(\tau)\int_{\tau}^{t}(t-u)\sigma(u)\,du\right]. \tag{68}$$

The cavity length $L_c(t)$ is determined for each moment by the equation:

$$S(t-L_c(t),t)=\frac{\pi}{4}. \tag{69}$$

An application of formula (68) has, naturally, restricted limits of applicability. However, the experimental tests justify its adequacy for a wide range of parameters.

3.3 EXPERIMENTAL CONFIRMATION OF THE INDEPENDENCE PRINCIPLE

The experimental test of the independence principle was carried out repeatedly and always gave good results. So, it was shown in the specially performed experiments [2] that in case of the model impact acceleration or stoppage, the cavity sections remote from the cavitator expanded some time in the same way as if the uniform motion continued.

Examples of calculation of the cavity shape at the variable cavitator velocity and also along the curvilinear trajectory are given there as well. The work [30] presents results of experimental testing the calculation of the unsteady cavity past the disk with periodically varying angle of slope. A comparison of the experimental and calculated cavity shape at the vertical water entry of bodies is given there as well.

A number of methodical experiments on testing the independence principle was carried out at the IHM UNAS including experiments at very high velocity of the models [31].

Fig. 18 shows a sequence of motion-picture frames of the deformation of the cavity caused by rapid reducing the cavitator drag without changing the cavitator diameter. The experiment was performed in the hydro-tunnel at the free-stream velocity V_∞ = 8.9 m/sec, the diameter D_n of the cavitator with variable drag [22] was equal to 20 mm. In the frames, a well expressed "stepped" boundary separating the initial and new-formed cavity parts is observed. This boundary moved with velocity V_∞ in full accordance with the independence principle.

We confirmed the independence principle validity at the very high velocity of motion in the special experiments on passage of the supercavitating model through a solid steel sheet with thickness 1.5 mm and through a hollow obstacle filled by air as well.

Fig. 19 shows a sequence of motion-picture frames of the process of the model passage through the thin steel sheet. The motion velocity is V = 1000 m/sec, the cavitator diameter is D_n = 1.3 mm. One can see in the frames that the presence of the obstacle preventing the water motion in longitudinal direction did not influence on the cavity development past the obstacle. This testifies that:

1) the fluid motion near the slender supercavity occurs predominantly in radial direction;

2) the adjoining supercavity sections separating by the steel sheet develop in such way as in the case of a flow without the sheet;

3) the longitudinal gas motion together with the supercavity is absent. If not, it would cease at passing of the model through the steel sheet. It could influence on the supercavity development just past the obstacle.

The flow directed to the model motion direction was observed only after the cavity closure.

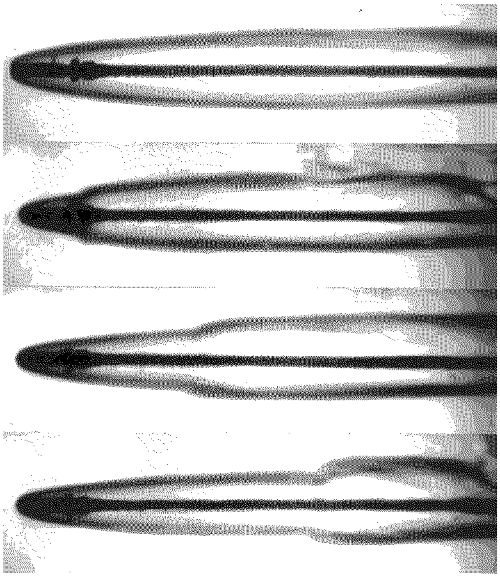

Fig. 18. Supercavity shape at rapid reducing the drag:

$D_n = 20$ mm, $V_\infty = 8.9$ m/sec

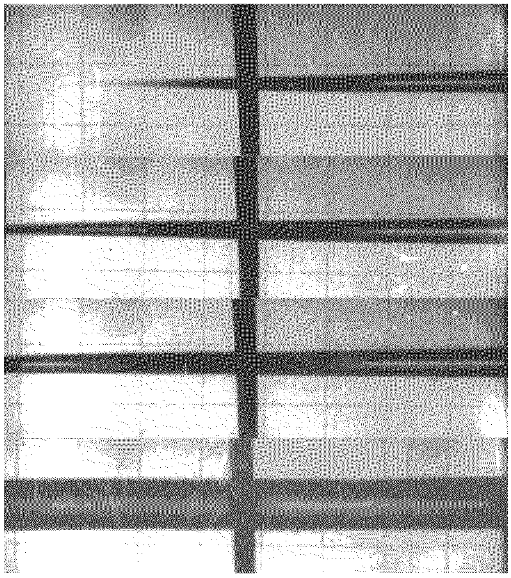

Fig. 19. Passing of supercavitating model through the obstacle:

$D_n = 1.3$ mm, $V = 1000$ m/sec

The experiment on passing of the supercavitating model through the hollow air space is especially demonstrative one. The obstacle represented a box with the frontal and back walls made of steel sheets having thickness 1 mm and the side walls made of glass having e thickness 10 mm (Fig. 20). In the experiment, we used the model with the length 280 mm and the cavitator diameter $D_n = 3.3$ mm.

A sequence of frames of shooting the experiments is given in Fig. 21. Passing through the complex obstacle containing the air space between the solid walls excluded the transition of both the pressure pulse and the velocity pulse in longitudinal direction. However, the cavity developed some time before and after the hollow box as if it was absent.

The presented sequences of frames visually demonstrate validity of the principle of independence of the cavity section expansion and, hence, adequacy of the approximate calculation method based on that principle.

4 Peculiarities of calculation of ventilated cavities

4.1 SIMILARITY PARAMETERS IN THE ARTIFICIAL SUPERCAVITATION

It follows from the above that the basic similarity parameters in artificial supercavitation are the cavitation number (1), the Froude number (3) and the dynamic parameter β (17). The cavitation number magnitudes in range $10^{-2} < \sigma < 0.1$ correspond to this type of flow.

The Froude number Fr characterizes the distorting effect of the gravity on the cavity shape. Estimations show that it is considerable when $\sigma Fr < 2$ [2].

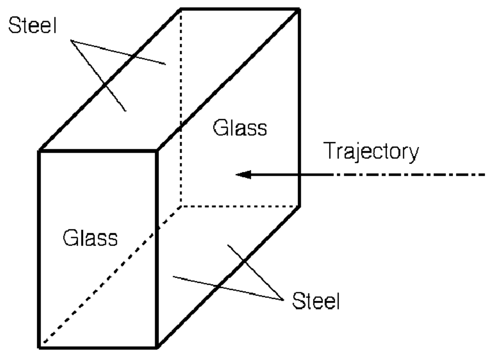

Fig. 20. Sketch of the hollow obstacle

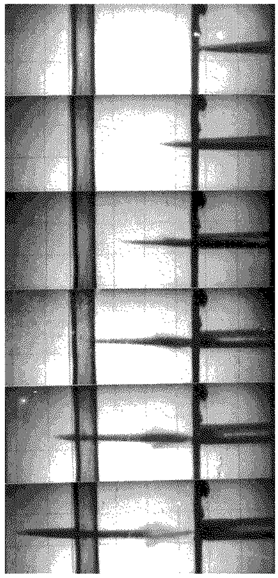

Fig. 21. Passing of supercavitating model through the air space: $D_n = 3.3$ mm, $V = 550$ m/sec

The parameter $\beta > 1$ characterizes the significance of elasticity of the gas filling the ventilated cavity. It is the basic similarity parameter at investigation of stability and unsteady behavior of gas-filled cavities [15]. When the parameter β increases, the gas elasticity significance increases as well. The ventilated cavities are stable when $1 \leq \beta < 2.645$ and unstable when $\beta > 2.645$.

In practice, it is impossible to attain simultaneous equality of all the numbers σ, Fr, β for the full-scale model and the bench testing one. That is why, investigation of scale effects (i.e. influences of different deviations from the similarity) is of importance in modeling the supercavitation processes.

We enumerate some possible causes of the scale effect at the physical modeling of the artificial cavitation flows.

1) **Influence of the flow boundaries.** The bench testing of the supercavitation flows usually are carried out in hydro-tunnels and hydro-channels in condition of the bounded flow. It is necessary to take into account the influence of the flow boundaries when the experimental data are recalculated to the motion in unbounded fluid.

The influence of the flow boundaries on the supercavity shape and dimensions has been well studied. The solid boundary closeness results in increasing the cavity dimension, and the free boundary closeness results in decreasing them at the same value of the cavitation number.

The influence of the flow boundaries on the gas rate coefficient is of importance in the case of ventilated cavities. It was shown experimentally that the approach to the free boundary results in decreasing the gas-leakage rate at the same values of σ and Fr [3, 10]. The influence of the cavity immersion depth on the gas-leakage coefficient at the second type of the gas-leakage was taken into account in the empirical formula (14).

2) **Influence of the gas flow in the cavity.** The experience shows that in the most of cases the influence of gas flow within the artificial cavity may be neglected. For steady cavities, it becomes considerable only in that cases when the gas flows in a narrow clearance between the body and the cavity wall. According to the Bernoulli equation the pressure in the clearance reduces, and the cavity boundaries may be deformed negatively. In this case local deformation of the cavity wall may be approximately calculated by the perturbation method [32].

3) **Supercavities in a bubble flow.** A peculiar scale effect may arise in the case of the gas-liquid bubble flow around the supercavitating bodies. We showed experimentally and theoretically that the supercavities can absorb gas from the two-phase bubble flow [33].

When the gas concentration is sufficient, this process causes to the considerable gas supply into the cavity and, as a result, to increasing the cavity dimension.

4.2 TAKING INTO ACCOUNT OF GRAVITY EFFECT

As was said above, the gravity effect on the horizontal supercavity consists in:

1) the cavity axis deformation upwards (floating-up of the cavity tail);
2) the cavity section shape deformation.

The cavity axis deformation in ponderable fluid is the main and greatest perturbation of the cavity.

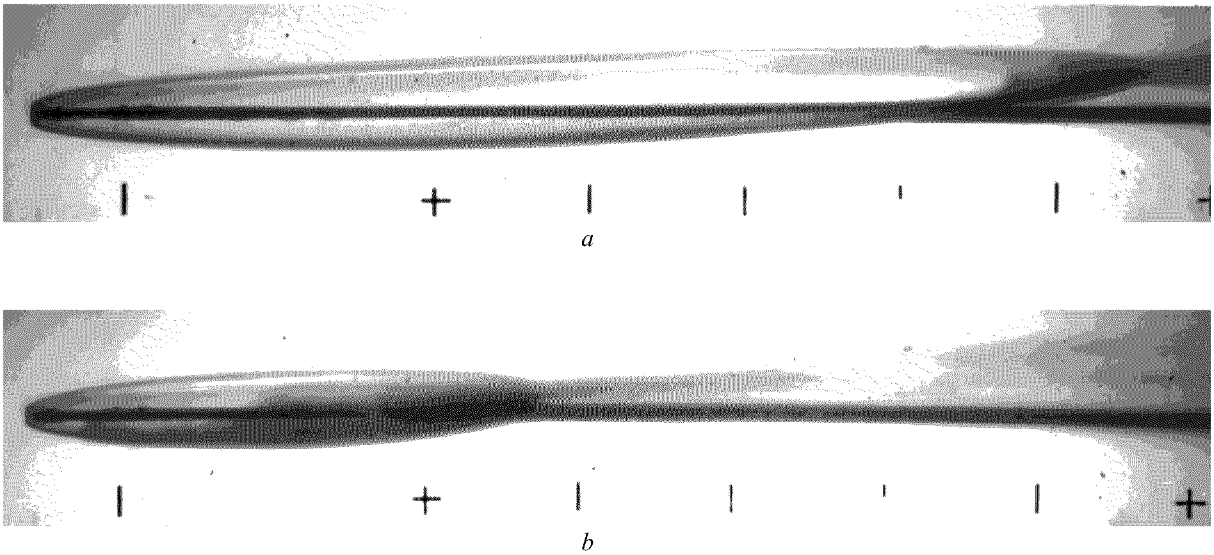

Fig. 22. View of the ventilated supercavities: V_∞ = 8.9 m/sec, Fr = 24.5; *a* - σ = 0.0334, *b* - σ = 0.0644

Fig. 22 demonstrates photographs of ventilated cavities at the same Froude number and the different cavitation numbers. The first form of the gas leakage from the cavity was observed in both cases.

In the works [31, 33] these deformations have been investigated in detail by the perturbation method.

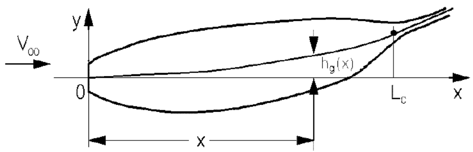

Fig. 23. Scheme of a supercavity in ponderable fluid

However, for practical calculations it is usually enough to evaluate the axis deformation in the first approximation by the theorem of momentum [2]. The calculation scheme is presented in Fig. 23.

We consider the balance of the cavity length element with the radius $R(x)$. Its momentum $\rho\pi R^2 V_\infty \dot{h}_g$ must be equal to the buoyancy force $\rho g Q$. Thus, we have:

$$\dot{h}_g(x) = \frac{gQ(x)}{\pi V_\infty R^2(x)}.$$

Integrating this equation along the x-axis, we obtain

$$h_g(x) = \frac{g}{\pi V_\infty}\int_0^x \frac{Q(s)}{R^2(s)}ds. \tag{70}$$

Here, $Q(x)$ is the cavity part volume from 0 to x, $R(x)$ is the current cavity radius.

In the work [33], the simple approximate formula was obtained for the axis deformation caused to the gravity effect:

$$h_g(x) = \frac{(1+\sigma)x^2}{3Fr_l^2}, \quad Fr_l = \frac{V_\infty}{\sqrt{gL_c}}. \tag{71}$$

Here, Fr_l is the Froude number with respect to the cavity length. Formula (71) may be used in ranges $0.05 \le \sigma \le 0.1$, $2.0 \le Fr_l \le 3.5$. Fig. 24 gives a comparison of calculation by formulae (70) (curve 1) and (71) (curve 2) with the experimental data [30]. Different marks correspond to different experimental conditions.

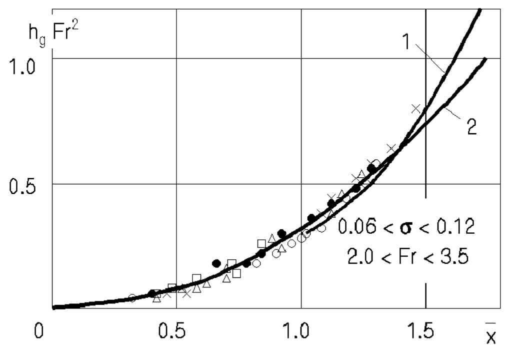

Fig. 24. A supercavity axis deformation in ponderable fluid

Deformation of the cavity section shape in the cross gravity field was investigated by the perturbation method in the works [30, 32]. The calculations showed and the experiments confirmed that a liquid crest with top directed up into the cavity is formed at the bottom cavity wall in this case. The crest height increases from the cavitator to the tail. Sometimes, this crest is small even at the cavity end. In other cases the crest top may attain the upper cavity wall and divide cavity on two tubes just past the mid-section (see Fig. 25)

A criterion of the gravity effect on the supercavity was obtained by theoretical way in the work [32]:

$$\nu = \sigma\sqrt{\sigma}Fr^2 \ge 1.5. \tag{72}$$

When this condition is fulfilled, the cavity is not destroyed, and the water crest does not close up with its upper wall even at the cavity end. With approaching the parameter ν to the limiting magnitude $\nu = 1.5$, two vortex tubes become the more expressed at the cavity end.

A comparison with the experiment showed that the criterion (72) is the more exact than the Campbell-Hilborne criterion (15). Indeed, we have σFr =0.82 < 1; ν = 3.73 > 1.5 for the experiment in Fig. 22, a. For the experiment in Fig. 22, b, we have σFr = 1.58 > 1; ν = 9.82 > 1.5. Thus, in the first case the Campbell-Hilborne criterion does not allow confidently to determine the gas-leakage type. Simultaneously, the criterion (72) determines the portion gas-leakage.

It is possible to determine the following intervals of changing the parameter ν that correspond to different levels of perturbation caused by gravity:

1) interval ν = 1 ÷ 2 is characterized by high level of perturbation, when the cavity past the mid-section transforms into the vortex tubes;

2) interval ν = 2 ÷ 4 corresponds to the moderate or considerable level of perturbation. In this case the water crest height is lower than the unperturbed cavity radius, although may be close to it.

3) interval ν = 4 ÷ 10 is characterized by weak level of perturbation. The gravity effect may be neglected at all when ν > 10.

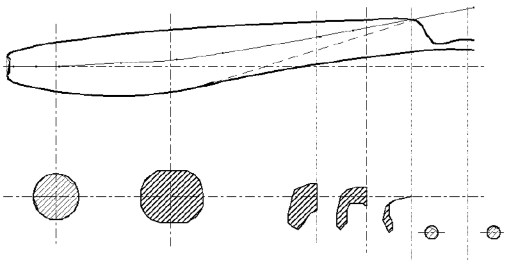

Fig. 25. Deformation of a ventilated supercavity axis in ponderable fluid

Fig. 26 represents the calculation by the perturbation method of the cross cavity section shapes when σ = 0.06, Fr = 10.0 [33]. In this case ν = 1.47. The dimensionless coordinate $\bar{x} = 2x/L_c$ was used at the calculation. In the sections $\bar{x}$ = 0.25 and $\bar{x}$ = 0.50 the gravity effect does not yet become apparent, in the section $\bar{x}$ = 0.75 the small compression from the bottom is appreciable. In the cavity mid-section $\bar{x}$ =1.00 the section shape differs from the circular one. When $\bar{x}$ = 1.25, the deformation is considerable. On the bottom it is close to the half of the cavity radius. The crest directed to up is well visible. The cavity is destroyed in the next sections.

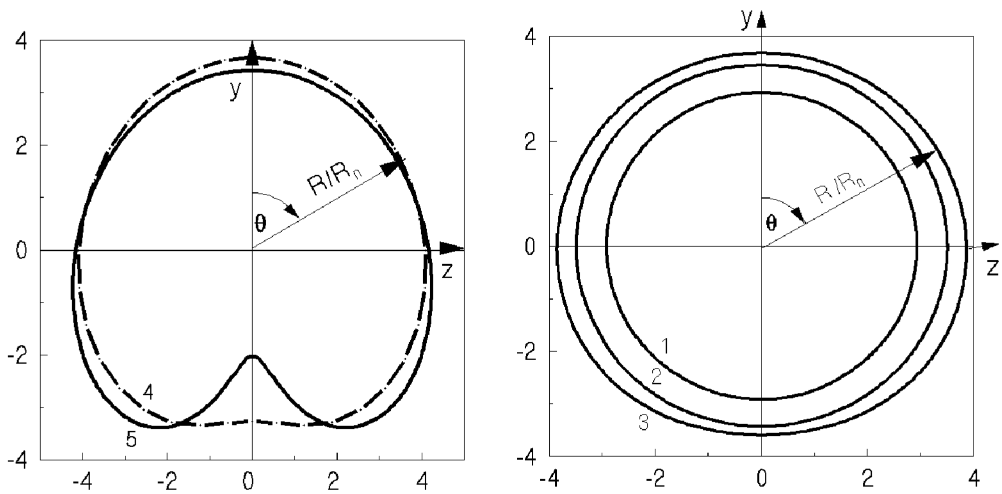

Fig. 26. Gravity effect on the cross cavity section shape: σ = 0.06, Fr = 10.0
1 - $\bar{x}$ = 0.25, 2 - $\bar{x}$ = 0.50, 3 - $\bar{x}$ = 0.75, 4 - $\bar{x}$ = 1.00, 5- $\bar{x}$ = 1.25

4.3 TAKING INTO ACCOUNT OF ANGLE OF ATTACK

The transverse force F_y arising on the cavitator non-symmetric about the free-stream results in the cavity axis deformation (Fig. 27). According to the theorem of momentum, the impulse of the transverse force on the cavitator must correspond to change of the momentum in the wake that is the same by magnitude and opposite by direction. This means that if the force on the cavitator is directed to up, then the cavity axis must be deflected to down (see Fig. 27) and vise versa.

Applying the theorem of momentum allows to estimate easily this bend [1]. The impulse $F_y\, t$ must be equal to momentum of the cavity length unit $-\rho\pi R^2 V_\infty t\dot{h}_v$. Hence, we have:

$$\dot{h}_f(x) = -\frac{F_y}{\rho\pi V_\infty^2 R^2(x)}.$$

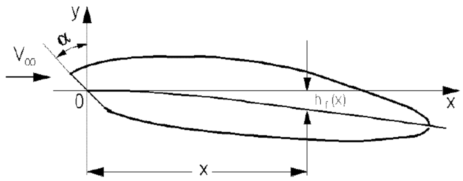

Fig. 27. Scheme of a supercavity past an inclined cavitator

Integrating this equation along the x-axis, we obtain

$$h_f(x) = -\frac{F_y}{\pi\rho V_\infty^2}\int_0^x \frac{ds}{R^2(s)}. \tag{73}$$

Components of the force acting on the cavitator-disk inclined to the stream with the angle α can be approximately calculated by formulae [1]:

$$F_x = F_{x0}\cos^2\alpha, \quad F_y = F_{x0}\sin\alpha\cos\alpha, \tag{74}$$

where F_{x0} is the disk drag when $\alpha = 0$. The formulae (74) well coordinates with experiment when $\alpha < 50°$. They may be applied not only for a disk but also for blunted cavitators of other shapes.

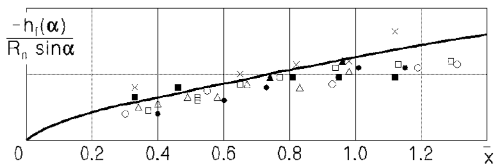

Fig. 28. A superavity axis deformation past the inclined cavitator: $\sigma = 0.08$, $\alpha = 33.5°$

An analysis of the cavitator orientation effect on the cavity shape using the perturbation method was given in the work [34]. As a result, the simple approximate formula was obtained to determine the cavity axis deformation under action of the lift on the cavitator:

$$h_f(x) = -c_y R_n\,(0.46 - \sigma + \bar{x}), \quad c_y = \frac{8F_y}{\rho V^2 \pi D_n^2}, \tag{75}$$

where $\bar{x} = 2x / L_c$. Fig. 28 gives a comparison of the calculation by the formula (75) with the experimental data [31].

Comparing the formulae (74) and (78), we can see that the cavity axis bend caused by the gravity increases according to the quadratic law, and one caused by the lift on the cavitator increases according to the linear law. Therefore, it is impossible to neutralize the gravity effect using the inclined cavitator along the whole cavity length.

In skewed stream, the cross cavity sections also are deformed. Since a projection of the inclined disk on the vertical plane is an ellipse, then the cross cavity sections before the mid-section will be elliptic with ratio of the half-axes

$$\frac{R_y}{R_z} = \cos\alpha. \tag{76}$$

In this case, the average radii in the middle cavity part before the mid-section are approximately equal to:

$$R(x) = R_0(x)\cos\alpha, \tag{77}$$

where R_0 is the radius of axisymmetric unperturbed cavity [2].

The simple formulae (71), (75) may be used for approximate calculation of both the stationary and non-stationary supercavities (using the independence principle). They are very convenient for using in codes for computer simulation of the cavitation flows.

4.4 EQUATION OF THE MASS OF GAS IN THE CAVITY BALANCE

The mathematical model of the unsteady ventilated cavity must include the equation of the mass of gas in the cavity balance [15]:

$$\frac{dm_g}{dt} = \dot{m}_{in} - \dot{m}_{out}, \tag{78}$$

where $m_g(t) = \rho_g(t)Q(t)$ is the mass of gas in the cavity; $Q(t)$ is the cavity volume; ρ_g is the density of gas in the cavity; $\dot{m}_{in}$ and $\dot{m}_{out}$ are the mass rates of the gas blowing into the cavity and carrying away from the cavity, respectively. Owing to the water thermal capacity, the process of the gas expansion in the cavity usually may be considered as isothermal one:

$$\rho_g(t) = C p_c(t), \tag{79}$$

where C is the constant. Taking the relation (79) into account, we rewrite the equation of the mass of gas in the cavity balance in the form:

$$\frac{d}{dt}[p_c(t)Q(t)] = p_\infty\left[\dot{Q}_{in} - \dot{Q}_{out}(t)\right], \tag{80}$$

where $\dot{Q}_{in}$ is the volumetric air-supply rate referred to the ambient pressure p_∞; $\dot{Q}_{out}(t)$ is the volumetric air-leakage rate from the cavity. The cavity pressure $p_c(t)$ is assumed to change synchronously along the cavity length.

Strictly speaking, the Eq. (80) may be applied when the parameters change not very rapidly. Really, the pressure perturbations $p_c(t)$ extend along the cavity with the sound speed in the vapor-gas medium filling the cavity a_g. Characteristic time of changing the pressure in the cavity with length L_c is equal: $T_1 = L_c / a_g$. Let the characteristic frequency of the unsteady process is f Hz. Then, supposition about the synchronism of changing the pressure along the cavity is equivalent to the inequality $T_1 << 1/f$. From

here we derive estimations for both the admissible frequency of the process and the dimensionless Strouhal number (10):

$$f << \frac{a_g}{L_c}, \qquad Sh << \frac{a_g}{V_\infty}. \tag{81}$$

The cavity pressure is constant in the case of the natural vapor supercavity, i.e. σ = const. Therefore, the Eq. (80) becomes needless.

In practice, we usually have $\dot{Q}_{in}$ = const. The value of the gas-leakage from the cavity $\dot{Q}_{out}$ depends on both the cavitation number and the Froude number and on a number of other factors as well [3, 6]. It is obvious for steady ventilated cavity that $\dot{Q}_{in} = \dot{Q}_{out}$.

The function $\dot{Q}_{in}(t)$ is given, and $\dot{Q}_{out}(t)$ is an unknown time function in problems of the ventilated cavities control by regulating the gas supply. As has been said yet, determining the form of function $\dot{Q}_{out}(t)$ for the concrete flow conditions is the most difficult problem of the artificial cavitation theory.

Conclusion

The described approximate mathematical model of the unsteady axisymmetric cavity is very convenient to develop fast calculation algorithms and codes permitting to perform computer experiments with dynamic display of the unsteady cavity shape and other necessary information on the computer screen immediately during run-time. The existing methods of "exact" numerical calculation of the unsteady supercavities are useless for these purposes due to their awkwardness and long run-time. Accuracy of the obtained results is established by direct comparison with experiment.

In our next lecture, results of computer simulation of the unsteady supercavitation processes of different types will be presented.

References

1. Birkhoff, G., Zarantonello, E.H., *Jets, Wakes and Cavities,* Academic Press Inc. Publishers, New York, 1957.

2. Logvinovich, G.V., *Hydrodynamics of Flows with Free Boundaries,* Halsted Press, 1973.

3. Epshtein, L.A., *Methods of Theory of Dimensionality and Similarity in Problems of Ship Hydromechanics,* Sudostroenie Publishing House, Leningrad, 1970 [in Russian].

4. Knapp, R.T., Daily J.W., Hammitt, F.G., *Cavitation*, McGraw-Hill, New-York, 1970.

5. Gorshkov, A.S., Rusetski, A.A., *Cavitation Tunnels,* Sudostroenie Publishing House, Leningrad, 1972 [in Russian].

6. Yegorov, I.T., Sadovnikov, Yu.M., Isayev, I.I., Basin M.A., *Artificial Cavitation,* Sudostroenie Publishing House, Leningrad, 1971 [in Russian].

7. Sedov L.I. *Mechanics of Continuum. Vol. 2.,* Nauka Publishing House, Moscow, 1976 [in Russian].

8. Silberman, E., Song, C.S., Instability of Ventilated Cavities, *J. of Ship Res.*, 1961, **5,** No. 1, pp. 13-33.

9. Michel, J.M., Ventilated Cavities. A Contributian to the Study of Pulsation Mechanism, *Unsteady Water Flow with High Velocities, Proc. of Int. Symposium IUTAM,* Nauka Publishing House, Moscow, 1973.

10. Epshtein, L.A., Characteristics of Ventilated Cavities and Some Scale Effects, *Unsteady Water Flow with High Velocities, Proc. of Int. Symposium IUTAM,* Nauka Publishing House, Moscow, 1973.

11. Epshtein, L.A., On Mechanism of Pulse Processes in End Zone of Attached Cavities, *Proc. of Symp. on Physics of Acoustic-Hydrodynamic Phenomena*, Nauka Publishing House, Moscow, 1975 [in Russian].

12. Levkovsky, Yu.L., *Structure of Cavitation Flows*, Sudostroenie Publishing House, Leningrad, 1978 [in Russian].

13. Cox, R.N., Clayden, W.A., *Air Entraiment at the Rear of a Steady Cavity*, Cavitation in Hydrodynamics, London, 1956.

14. Campbell, I.J., Hilborne, D.V., Air Entrainment behind Artificially Inflated Cavities, *Second Symposium on Cavitation on Naval Hydrodynamics,* Washington, 1958.

15. Paryshev, E.V., Theoretical Investigation of Stability and Pulsations of Axisymmetric Cavities, *Trudy TsAGI,* 1978, No. 1907, pp. 17-40 [in Russian].

16. Lapin, V.M., Epshtein, L.A., On Gas Leakage Caused by Cavity Pulsation, Uchenye Zapiski TsAGI, **15**, No. 3, pp. 23-30 [in Russian].

17. Gurevich, M.I., *Theory of Jets in Ideal Fluid.* 2nd Edition, Nauka Publishing House, Moscow, 1979 [in Russian].

18. Migirenko, G.S., Kozyuk, G.S., Maltsev, V.I., Novikov, B.G., Some Methods of Control of Cavitation Flow at Low Magnitudes of Froude numbers, *Unsteady water flow with high velocities, Proc. of Int. Symposium IUTAM,* Nauka Publishing House, Moscow, 1973 [in Russian].

19. Maltsev, L.I., Migirenko, G.S., Mikuta, V.I., Cavitation flows with Cavity Closure on Fluid Jet, In: *Investigations on Developed Cavitation*, In-t of Thermal Physics, Novosibirsk, 1976 [in Russian].

20. Terentiev, A.G., Dimitrieva, N.A. Theoretical Investigation of Cavitating Flows, *Proc. of Third International Symp. on Cavitation*, Grenoble, France, 1998, Vol. 2, pp. 275-280.

21. Garabedian, P.R., Calculation of axially symmetric cavities and jets. *Pac. J. Math.,* 1956, **6**, No. 4, pp. 611-684.

22. Savchenko, Yu.N., Vlasenko, Yu.D., Semenenko, V.N., Experimental study of high–speed cavitated flows, *Int. J. of Fluid Mechanics Research,* 1999, **26**, No. 3, pp. 365-374.

23. Guzevsky, A.G., *Numerical Analysis of Cavitation Flows*, Preprint of In-t of Thermal Physics, Novosibirsk, 1979, pp. 40-79 [in Russian].

24. Guzevsky L.G., Approximation Dependencies for Axisymmetric Cavities past Cones, In: *Hydrodynamic Flows and Wave Processes,* In-t of Thermal Physics, Novosibirsk, 1983, pp. 82-91 [in Russian].

25. Adams, M.C., Sears, W.R., Slender Body Theory. Review and Extensions, *J. of Aeron. Sci.*, 1953, **20**, No. 2., pp. 85-98.

26. Ashley, H., Landahl, M., *Aerodynamics of Wings and Bodies,* Addison-Wesley Publ. Co. Inc., 1968.

27. Grigoryan, S.S., Approximate Solution on Separated Flow around Axisymmetric Body. *Prikladnaya matematika i mehanika,*1959, **23,** No. 5, pp. 951-953 [in Russian].

28. Yakimov, Yu. L. On Axially Symmetric Separated Flow around a Body of revolution at Small Cavitation Numbers, *Prikladnaya matematika i mehanika,* 1968, No. 32, pp. 499-501 [in Russian].

29. Logvinovich, G.V., Serebryakov, V.V., On Methods of Calculating a Shape of Slender Axisymmetric Cavities, *Gidromehanika,* 1975, No. 32, pp. 47-54 [in Russian].

30. Zhuravlyov, Yu.F. Methods of Theory of Perturbations in 3D Jet Flows, *Trudy TsAGI,* 1973, No. 1532, pp. 8-12 [in Russian].

31. Savchenko, Yu.N., Semenenko, V.N., Putilin, S.I., Unsteady Supercavitated Motion of Bodies, *Int. J. of Fluid Mechanics Research*, 2000, **27,** No. 1., pp. 109-137.

32. Buyvol, V.N., *Slender Cavities in Flows with Perturbations*, Naukova Dumka Publishing House, Kiev, 1980 [in Russian].

33. Savchenko, Y.N., Semenenko, V.N., The Gas Absorption into Supercavity from Liquid-Gas Bubble Mixture, *Proc. Third Internat. Symp. on Cavita-tion.* Grenoble, France, 1998, Vol.2, pp. 49-53.

34. Logvinovich, G.V., Buyvol, V.N., Dudko, A.S., et al, *Free Boundary Flows*, Naukova Dumka Publishing House, 1985 [in Russian].